Polymer Bulletin (2023) 80:9217–9236
https://doi.org/10.1007/s00289-022-04500-y

ORIGINAL PAPER

Elaboration and characterization of new adsorbents based on conducting PANI/zeolite HY/TiO_2 nanocomposite applied for chromate adsorption

Z. Ghebache[1] · Z. Safidine[2] · F. Hamidouche[3] · N. Boudieb[3] · A. Benaboura[1] · M. Trari[4]

Received: 25 February 2022 / Revised: 9 September 2022 / Accepted: 28 September 2022 /
Published online: 10 October 2022

Abstract

The preparation of polyaniline/HY/TiO_2 *p–n* heterojunction/polymer is successfully performed by in situ chemical polymerization of aniline doped by 5 w% of HY zeolite (acid solid) using persulfate $(NH_4)_2S_2O_8$ as oxidant in aqueous solution containing 5 to 20 wt% of TiO_2 with respect to aniline monomer quantity. The product is characterized by X-ray diffraction (XRD), FT-IR spectroscopy, SEM analysis, thermal gravimetry, UV–visible diffuse reflectance and electrical conductivity. The FT-IR spectra revealed the presence of TiO_2 and PANI as a main matrix in nanocomposites while the XRD patterns show that the diameter of PANI/HY/TiO_2 lies between 20 and 70 nm. In the second part, we investigate the effect of the physical parameters on the equilibrium adsorption of chromate Cr(VI) on PANI/HY/TiO_2 nanocomposites. The adsorption characteristics of the composite toward Cr(VI) are followed by atomic absorption spectroscopy (AAS). The effect of contact time, sorbent size and Cr(VI) initial concentration (C_o) on the Cr(VI) uptake is also studied. It has been observed that the capacity of Cr(VI) adsorption on PANI/HY/TiO_2 increases with increasing C_o while the PANI/HY/5TiO_2 has a larger uptake capacity. The isotherm data are well fitted with the Langmuir isotherm model with maximum adsorption capacity of 454.54 mg/g. The calculated thermodynamic parameters showed that the Cr(VI) adsorption onto PANI/HY/5TiO_2 is endothermic ($\Delta H^\circ = 12.478$ kJ/mol) and spontaneous ($\Delta G^\circ_{300\,K} = -11.186$ kJ/mol).

Keywords Nanocomposite conductor · Polyaniline · TiO_2 anatase · Zeolite HY · Chromate · Adsorption

✉ M. Trari
solarchemistry@gmail.com

Extended author information available on the last page of the article

Introduction

Nanocomposites of conductive polymers and inorganic nanoparticles are attracting more and more attention not only because they combine the advantageous properties of conductive polymer and inorganic particles but also because of new types of composite materials with synergistic or complementary behaviors, with interesting physical properties and many potential applications [1–6]. Polyaniline, one of the most intensively studied conducting polymers over the last years, has attracted considerable attention for the preparation of its composites with inorganic compounds. One can cite the transport and magnetic properties of $Cu_{0.4}Zn_{0.6}Cr_{0.5}Sm_{0.06}Fe_{1.44}O_4$/polyaniline nanocomposites [7], polyaniline–molybdenum trisulfide composite [8], polyaniline nanofibers [9] and polyaniline V_2O_5 composite [10], TiO_2, SnO_2, WO_3, ZnO, Nb_2O_5, In_2O_3 and others [11–16].

Zeolites are nanoporous aluminosilicates in which the presence of Al introduces charge defects that are compensated by non-framework cations. These acid solids are usually synthesized in the presence of Na^+, but as this ion is readily exchangeable, a large variety of exchanged zeolites have been generated for the catalysis, adsorption and ion-exchange purposes [17], These considerations prompted us to investigate a commercial zeolite Y in its hydrogenated form (zeolite HY) for the removal of simazine from water. Indeed, the use of zeolites in the environment protection is already known [18, 19]. Furthermore, zeolite Y is (i) inexpensive and therefore commercially available; (ii) exhibits only one type of windows with smallest dimension of 0.74 nm [20]: the molecule (length 1.034 nm, width 0.749 nm [21]) thus appears to be able to enter the porous system, possibly ensuring a rapid uptake [22]. Moreover, the acidity of the zeolite surface implies a good adhesion with the conducting polymer, with an easy charge carrier transport through the cell, thus minimizing the internal resistance and maximizing its efficiency. Besides, the intercalation of a conducting polymer into a porous and leafy material, like zeolite, protects the former from degradation [23].

On the other hand, TiO_2 has versatile properties with various applications in photovoltaic, photocatalysis and environmental protection [24–26], it is relatively inexpensive, non-toxic and possesses promising photoelectric properties. However, its band gap ($E_g \sim 3.2$ eV) is wide and limits the exploitation of sunlight since only ~ 4% falls in the UV range [27–29]. It was found that the nanosized *p*–*n* heterojunction, i.e., *p*-type PANI zeolite HY/*n*-type TiO_2 works as a switch to control the electric current flow in TiO_2 microfibers [30].

On the other hand, heavy metals are potentially hazardous to human health even at low concentrations. Chromium is used in industries such as electroplating, tanning, textile and thus is widely present in the effluents of these industries. It is commonly found in two oxidation states; hexa- and trivalent states Cr(III)) and trivalent Cr(VI). The latter is about 500 times more toxic to aquatic life than the trivalent state [31] and various methods were used for its removal, including chemical precipitation, reverse osmosis, ion exchange and adsorption [32–34].

In this study, polyaniline was synthesized using doped acid solid HY zeolite in the presence of TiO_2 at different percentages (5–20 w%). PANI/HY/TiO_2

nanocomposite was tested as adsorbent for Cr(VI) reduction from aqueous solutions under various conditions. The adsorption time and Cr(VI) concentration were tested and the equilibrium isotherms were investigated.

Experimental methods

Materials

The aniline (purity > 99%) was purchased from Merck, zeolite NH_4Y [$Na_1(NH_4)_{52.33}Al_{53.33}Si_{138.6\,7}O_{384}$], Zeolist International, $SiO_2/Al_2O_3 = 5.2$; $Na_2O = 0.2\%$, Si/Al = 2.6 (ZEOLIST®). The anatase TiO_2 nanoparticles (size: 20–70 nm) were obtained from Biochem, $(NH_4)_2S_2O_8$, APS) (Panreac 99%), ammonia solution (25% Biochem), methanol (Analar Normapur, *N*-methyl-2-pyrolidone Biochem).

Characterization

The FT-IR spectra were obtained with a Shimadzu 8400S spectrometer (resolution: 1 cm^{-1}); the measurements were performed in absorption mode using KBr pellets (spectroscopic grade). The UV–visible spectra of the deprotonated samples dissolved in *N*-methyl-2-pyrrolidone (NMP) were recorded using a UV–Vis Spectrophotometer Shimadzu UV-2401 in the range (290–900 nm). The electrical conductivity was measured at ambient temperature on pressed pellets using the Four-Point Probe (Jandel Engineering RM3000) with a DC current source. The thermal stability of the sample was performed on a thermogravimetric analyzer (Model: TG 209 F1 NETZSCH German) at a heating rate of 10 °C min^{-1}. The XRD patterns were recorded in the 2θ range (5–70°, step: 0.02°) with a PANalytical, X'PerPRO X-ray diffractometer while the morphological studies of composite samples were performed by SEM technique with scanning electron microscope (Model PHILIPS XL 30). Atomic absorption spectroscopy (AAS Absorption Spectrometer, Unicam SOLAAR 969) was used for the Cr(VI) titration.

Synthesis of PANI/HY/TiO_2 nanocomposite

Pure PANI was synthesized by in situ chemical oxidative polymerization (0–5 °C), which has been reported in detail elsewhere [35–37]. The composite PANI/HY/TiO_2 was synthetized by an in situ chemical oxidation polymerization of aniline using HY zeolite solid. HY was prepared by thermal treatment of NH_4Y [38] and $(NH_4)_2S_2O_8$ as oxidant in presence of colloidal TiO_2 nanoparticles, ranging (0–5 °C) in air. In a typical procedure, TiO_2 nanoparticles were suspended in distilled water and sonicated for 1 h to reduce the aggregation of TiO_2 nanoparticles. The aniline (0.1 M) was dissolved in 100 mL of water and then mixed with 10 mL of sonicated colloidal TiO_2 nanoparticles by further sonication for 30 min. 100 mL solution [$(NH_4)_2S_2O_8$/aniline = 1.5] was added dropwise

for a well dispersion (2 h) under continuous stirring at (0–5 °C). Good degree of polymerization was achieved after 3 h, and a dark green precipitate was recovered. The solution was left in undisturbed position overnight for the completion of chemical reaction; the precipitate was removed by filtration, washed repeatedly with distilled water and dried under vacuum for 24 h.

The different contents PANI/HY/TiO_2 nanocomposites were synthesized using 5, 10, 20 wt% to TiO_2 with respect to aniline monomer. The schematic diagram of the stepwise synthesis is shown in Fig. 1.

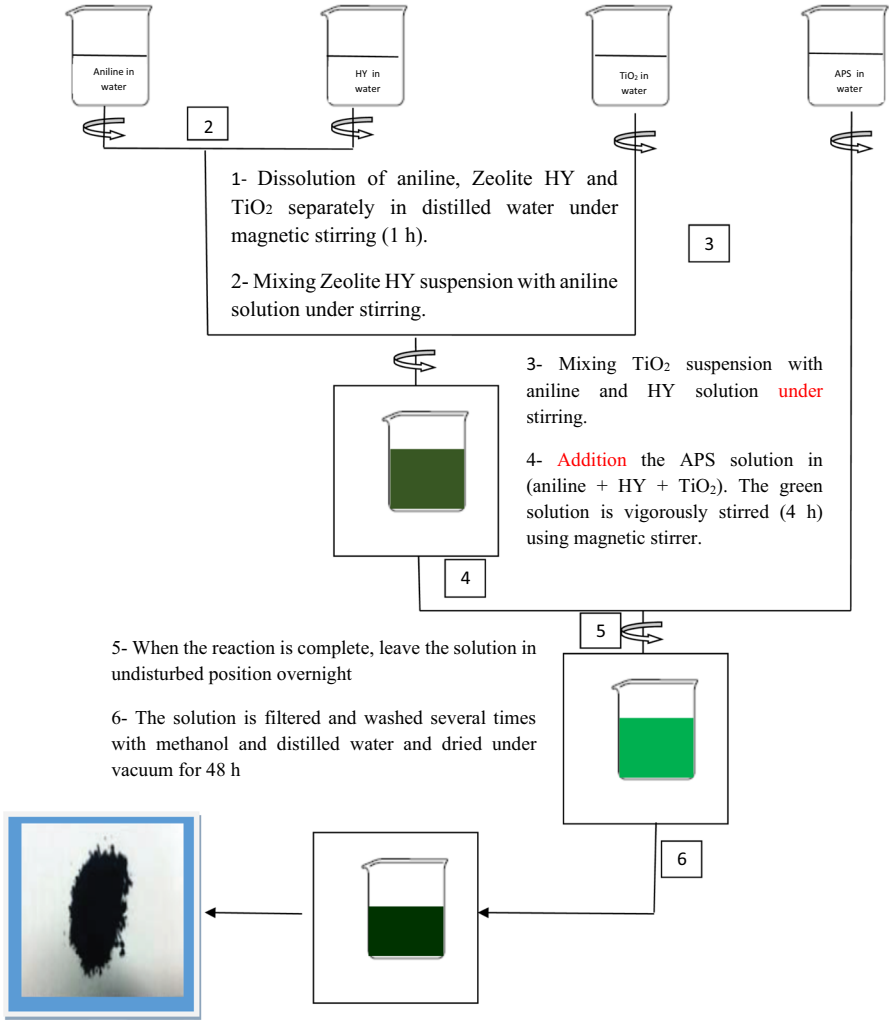

Fig. 1 Schematic diagram by steps for the synthesis of PANI/HY/TiO_2 nanocomposite using in situ oxidative polymerization

Adsorption experiments

To determine the conditions that achieve the maximum amount of Cr(VI) removal, adsorption experiments were done; the reaction isotherm and kinetics were also conducted in this study.

The Cr(VI) solutions were prepared at different concentrations (10–100 ppm) from a stock solution (1000 ppm) by dissolving extra pure K_2CrO_4 in water. The adsorption isotherm and kinetics were conducted in this study. Various amounts of nanocomposites PANI/HY/TiO_2 powder were introduced into 100 mL volumetric flasks to which 50 mL Cr(VI) solution at different concentrations were added. The adsorption tests were conducted at a fixed temperature of 30 °C; the efficiency of Cr(VI) removal was calculated as follows:

$$\text{Removal efficiency } (\%) = 100\left(\frac{C_i - C_f}{C_i}\right) \tag{1}$$

where C_i and C_f are the initial and final concentrations (ppm), respectively. The amount of metal adsorbed (q_i) per specific amount of adsorbent (mg/g) was obtained as follows:

$$q_i = \left(\frac{(C_i - C_f).v}{m}\right) \tag{2}$$

where C_i and C_f (ppm) are the liquid phase concentrations of solutes at initial and time t, v the solution volume (ml) and m the mass of composite (g).

Results and discussion

Infrared Spectroscopy

Figure 2 shows the FT-IR spectra of pure PANI, HY and PANI/HY/TiO_2 composite, in which some vibration bands are observed. The characteristic bands attributed to the emeraldine salt are 3464 and 3252 cm^{-1}, corresponding to stretching vibration of O–H and N–H [39, 40]. The band centered at 1575 cm^{-1} of quinonoid ring stretching and that at 1497 cm^{-1} of benzenoid ring stretching is related to C=C vibration of the system (N=Q=N) and system C–C (N–B–N) ring deformation, respectively. These two bands are important since they deliver qualitative information on the oxidation of polyaniline; the peaks 2909 and 2841 cm^{-1} are assigned to stretching vibrations of C–H coming from the PANI structure [41, 42]. The characteristic bands of the zeolite at 1135 and 1044 cm^{-1} correspond to the stretching group O–T–O and the elongation of the early group T–O–T [43, 44].

The FT-IR spectrum of TiO_2 (Fig. 2g) confirmed the existence of well-defined peaks at 660 and 505 cm^{-1} (< 1000 cm^{-1}), in good agreement with previously reported spectra of TiO_2 composite [44]. The strong peak of TiO_2 occurs in the

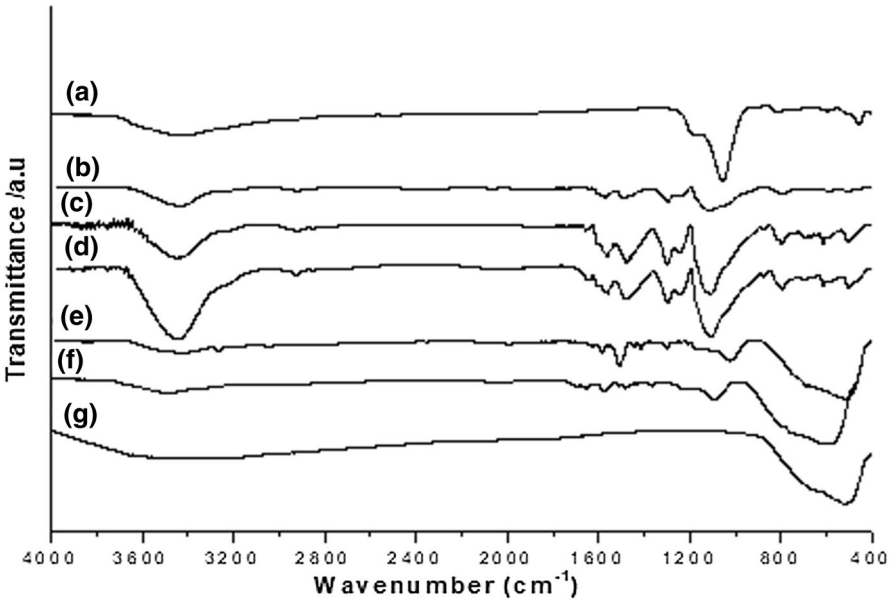

Fig. 2 FT-IR spectra of **a** pure PANI, **b** HY, **c** PANI/HY, **d** PANI/HY/5TiO_2, **e** PANI/HY/10TiO_2, **f** PANI/HY/20TiO_2 and **g** TiO_2 in the range (4000–400 cm^{-1})

composite with increasing the weight, indicating a strong interaction between PANI/HY and TiO_2.

Ultraviolet–visible spectroscopy

The UV–visible spectra of PANI, PANI/HY/5TiO_2, PANI/HY/10TiO_2, PANI/HY/20TiO_2 show two absorption maxima in NMP while the zeolite HY has no absorption (Fig. 3). The spectrum of PANI base has bands at 332 and 647 nm. The former is assigned to the electronic transition $\pi - \pi^*$ observed for standard PANI emeraldine base [46] and is sensitive to the number of aniline units (330–340 nm). The band at 647 nm corresponds to the excitation of the charge transfer from the highest occupied energy level (HOMO), centered on the benzenoid ring, to the lowest unoccupied energy level (LUMO), centered on the quinonoid ring [47, 48].

The UV–visible spectrum of the PANI/HY/TiO_2 composite exhibits two absorption bands, which show a blueshift with increasing the TiO_2 content in the composites: from 363 and 651 nm for PANI/HY/5TiO_2 to 347 and 647 nm for PANI/HY/10TiO_2, and 345 and 645 for PANI/HY/20TiO_2.

Thermal analysis

The TG plots of PANI, PANI/HY and PANI/HY/TiO_2 nanocomposites (Fig. 4) show the thermogravimetric analysis (TGA) of polyaniline and PANI/HY and PANI/

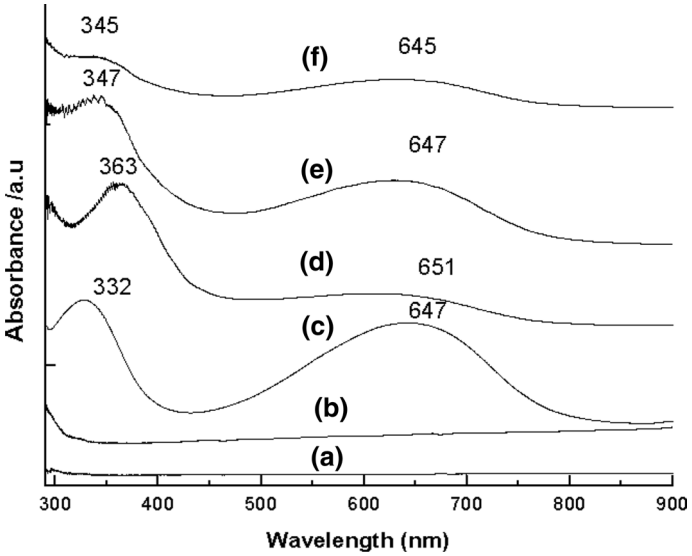

Fig. 3 UV–visible spectra of **a** HY, **b** TiO_2 and deprotonated from **c** PANI, **d** PANI/HY/5TiO_2, **e** PANI/HY/10TiO_2 and **f** PANI/HY/20TiO_2 in *N*-methyl-2-pyrrolidone

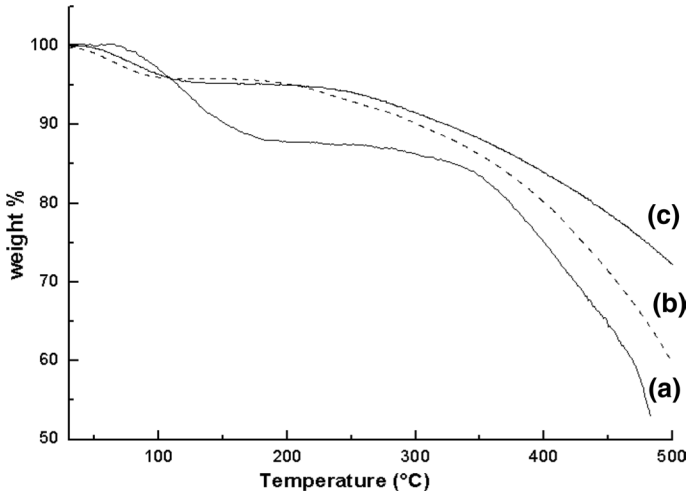

Fig. 4 TGA curves for PANI, 5HY, PANI/HY/5TiO_2, recorded under air stream at a heating rate of 5 °C min^{-1}

HY/5TiO_2 nanocomposite. PANI shows three-step thermal degradation process in the range (30–150 °C), (150–350 °C) and (350–500 °C) corresponding to the moisture and dopant losses and main chain degradation of PANI, respectively [49].

It should be noted that the weight loss follows a two-step manner in the nanocomposite, the removal of water molecules in PANI/HY (96 wt%) and PANI/HY /5TiO_2 (94 wt%). The residual weight (350–500 °C) corresponds to the degradation of the

main chain of PANI in PANI/HY 63 (wt%) and (74.34 w%) PANI/HY/TiO_2, and it is smaller than the extent of the thermal decomposition of PANI. The increased thermal stability of PANI in PANI/HY and PANI/HY/5TiO_2 composites is explained by the strong interactions PANI with zeolite HY, PANI and zeolite HY and TiO_2, which restrict thermal motion of PANI chains.

Electrical conductivity

In comparison with pure PANI/HY, the conductivity (σ_{300K}) of 5 wt% PANI/HY/TiO_2 composite increases from 1.12 to 2.2 S/cm (Fig. 5). This may be attributed to TiO_2 nanoparticles in PANI/HY matrix to form an efficient system for the charge transport between different molecular chains of PANI/HY, thus enhancing the conductivity of the composite. The decreased conductivity of 10 wt% PANI/HY/TiO_2 nanocomposite is due to the partial blockage of conductive path and reduction of conjugation length between PANI/HY chains by excess of TiO_2 nanoparticles in the PANI/HY matrix [50]. The σ value implies that the conduction occurs by small polaron lattice, assimilated to a heavy particle with a small mobility at 300 K and a limited free path.

X-ray diffraction (XRD)

Figure 6 presents the XRD patterns of TiO_2 nanoparticles, pure HY, PANI and PANI/HY/TiO_2 composites. It is apparent that the TiO_2 nanoparticles are crystalline and the positions of all the sharp peaks reveal an anatase crystalline polymorph (PDF≠01-071-1168 data file) in agreement with earlier reported data [51]. The 2θ peaks at 25.21, 36.82, 37.66, 38.45, 47.96, 53.77 and 54.98 correspond to the

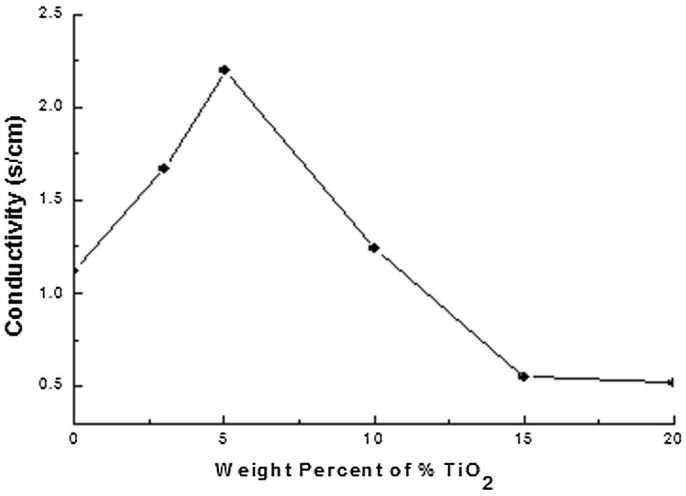

Fig. 5 Variation of the electrical conductivity (σ_{300K}) of PANI/HY/TiO_2 nanocomposite with different TiO_2 concentrations at room temperature

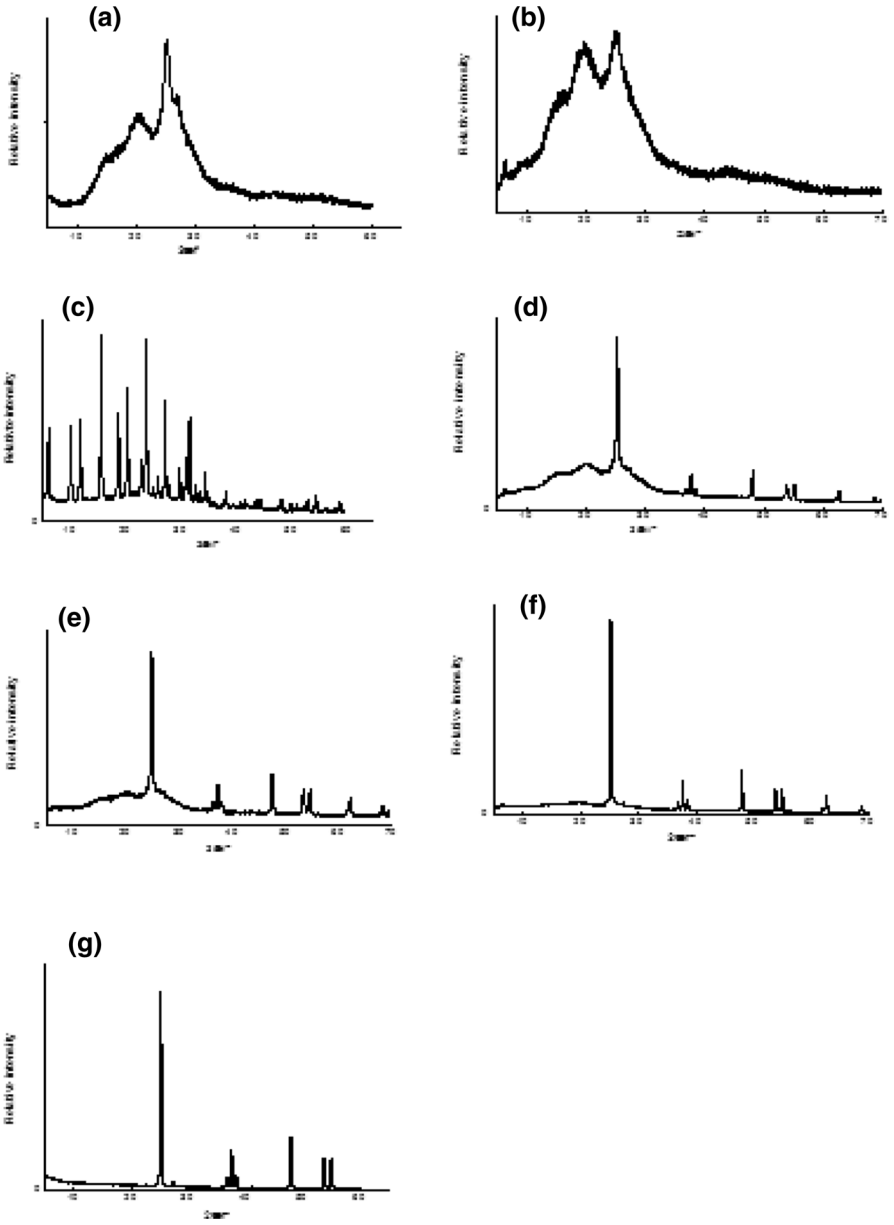

Fig. 6 XRD patterns of parent **a** pure PANI, **b** PANI/HY, **c** pure HY, **d** PANI/HY/5TiO_2, **e** PANI/HY/10TiO_2, **f** PANI/HY/20TiO_2, **g** pure TiO_2

inter-reticular planes (101), (103), (004), (112), (200), (105), (211). The other crystalline forms of TiO_2 (rutile and brookite) are not detected.

The average particles size (D) is calculated for the selected samples by using the full width at half maximum (FWHM = β, radian) (Fig. 7):

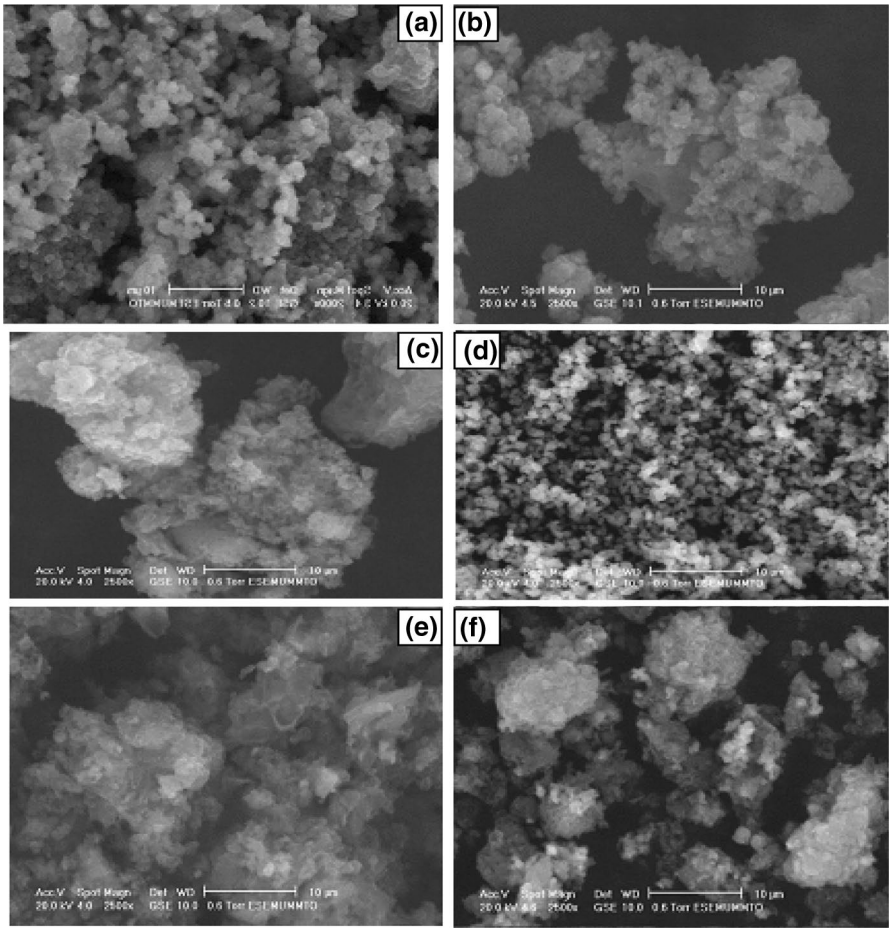

Fig. 7 SEM images of **a** HY, **b** pure PANI, **c** PANI/HY, **d** pure TiO_2, **e** PANI/HY/5TiO_2 and **f** PANI/HY/10TiO_2

$$D = \frac{K\lambda}{\beta \cos\theta} \tag{3}$$

where K is the shape factor for the average crystallite (~0.9), λ the X-ray's wavelength for Cu–K_α (=0.15418 nm). The calculated sizes based on the XRD data are found to be 50 nm for TiO_2 nanoparticles, 26 nm for nanocomposite content 5%TiO_2, 27 nm for 10% of TiO_2 and 66 nm for 20% of TiO_2. The results indicated that the encapsulated TiO_2 nanoparticles with PANI chains restrict the growth of PANI chains around TiO_2 nanoparticles. Assuming spherical crystallites, a minimal specific surface area of ~100 $m^2\ g^{-1}$ is evaluated from the relation $\{S = 6 \times (\rho_{exp} L)^{-1}\}$, ρ_{exp} is the experimental density (~2 g cm^{-3}) determined by pycnometry.

Scanning electron microscopy (SEM)

There is a clear evolution of the morphology with the PANI/HY aggregates of irregular shape and size. The study of prepared composite by SEM analysis indicates that PANI/HY/10TiO_2 shows rather homogeneous morphology in contrast to PANI/HY/5TiO_2 and PANI/HY, which are heterogeneous with a certain porosity, an attractive property for the Cr(VI) adsorption.

Metal adsorption

Effect of contact time

The saturation time of PANI/HY/5TiO_2, PANI/HY/10TiO_2, PANI/HY/20TiO_2 nanocomposites was obtained by plotting the removal efficiency of Cr(VI) against time. For a Cr(VI) concentration less than 50 ppm, the maximum was reached in a short period and the composite adsorbs completely the metal (100%) of PANI/HY/5TiO_2. The uptake kinetic is related to the specificity of the interaction with the polymeric matrix/Cr(VI).

Figure 8 shows the Cr(VI) elimination by PANI/HY/5TiO_2, PANI/HY/10TiO_2 and PANI/HY/20TiO_2 nanocomposite. The removal increases with time and reaches an equilibrium within 15 min. High Cr(VI) adsorption rates for the three nanocomposites are observed at the beginning, and then a plateau region is progressively reached within 15 min for an initial concentration of 50 ppm. In each case, the decreasing Cr(VI) concentration remained in solution indicates that chromate is strongly adsorbed onto PANI/HY/5TiO_2 comparatively with PANI/HY/10TiO_2 and PANI/HY/20TiO_2. The Cr(VI) recovery is of interest in terms of both environmental and economic effects.

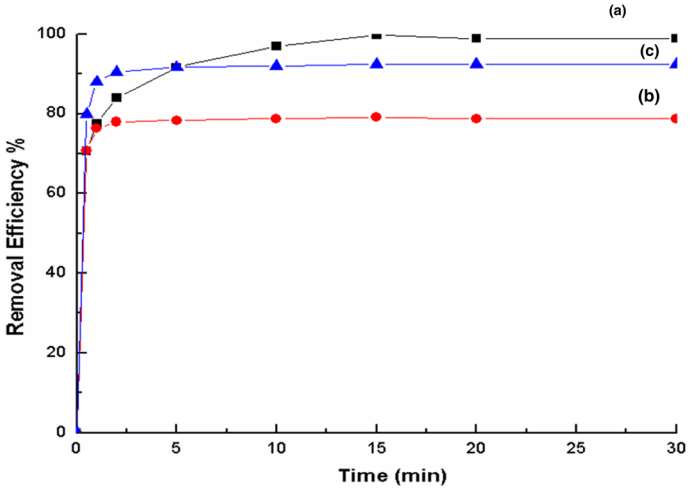

Fig. 8 The effect of contact time on the removal efficiency {C_o = 50 ppm, V = 50 mL and m = 0.2 g}. **a** PANI/HY/5TiO_2, **b** PANI/HY/10TiO_2 and **c** PANI/HY/20TiO_2

Effect of pH

The pH is a crucial parameter in the adsorption and its effect was studied in the range (2 – 12) at 30 °C for initial Cr(VI) concentration (C_o) of 50 mg/L on PANI/HY/5TiO_2; the results are shown in Fig. 9. It was observed that the pH strongly affects the uptake capacity of the adsorbent for Cr(VI) and the uptake capacity increases with augmenting pH, and peaks at pH 7.3 with an abatement of 99.7%, it decreases with increasing pH to 12. This is explained by attractive electrostatic forces between the negative charges of the catalyst surface and Cr(VI), which leads to better adsorption, thus favoring its elimination.

Effect of initial Cr(VI) concentration (C_o)

The effect of the initial Cr(VI) concentration (C_o) on the removal efficiency was studied in the range (10–100 ppm). At optimum pH and contact time, 0.2 g of PANI/HY/5TiO_2 was added to 100 mL of Cr(VI) solution at various concentrations. The results (Fig. 10) show that with increasing C_o, the amount of adsorbed Cr(VI) increases at equilibrium, a behavior due to the available adsorption sites, higher than the Cr(VI) in solution keeping in mind the high active surface area (~ 100 m^2 g^{-1}).

The adsorption capacity was found to increase with augmenting C_o. Higher concentrations provide increased driving force to overcome the mass transfer resistance of Cr(VI) between the aqueous and solid phases resulting in a higher probability of collision between Cr(VI) ions and sorbents. This suggests that the adsorption on PANI/HY/5TiO_2 shows strong adsorbate–adsorbent interactions.

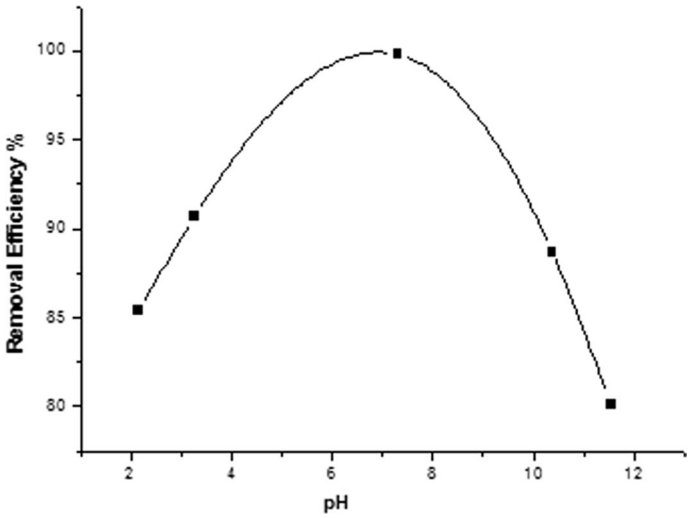

Fig. 9 Effect of pH on adsorption capacity of PANI/HY/5TiO_2 for Cr(VI) {C_o = 50 ppm, V = 50 mL and m = 0.2 g}

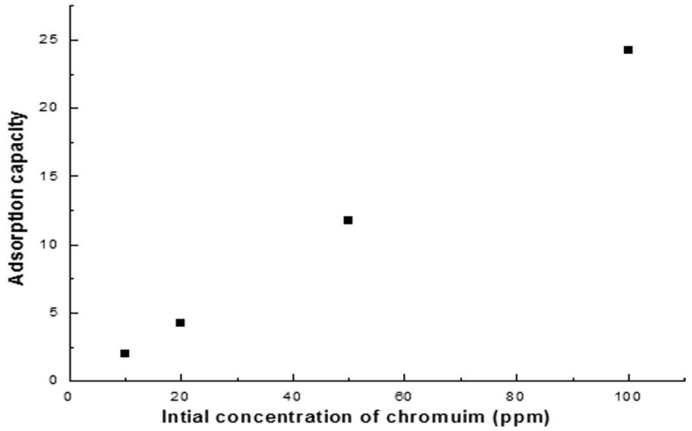

Fig. 10 The effect of initial Cr(VI) concentration (C_o) on the adsorption capacity {$V=50$ mL and $m=0.2$ g and time 15 min}

Effect of PANI/HY/5TiO$_2$ dose

The effect of sorbent dose was also investigated and different amounts (0.1–0.5 g) of sorbent were suspended in 50 mL Cr(VI) solution (50 ppm) under optimized conditions. It was observed that the adsorption percentage of Cr(VI) onto PANI/HY/5TiO$_2$ increases rapidly with increasing the adsorbent concentration (Fig. 11). This result is expected because the increase in adsorbent dose leads to greater surface area with more adsorption sites.

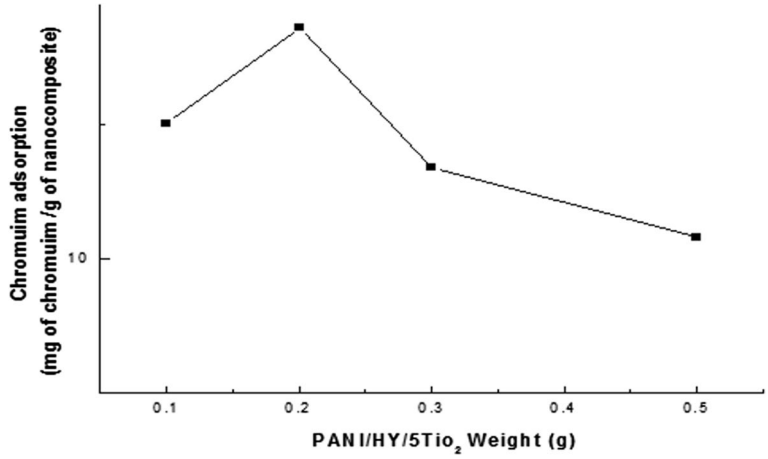

Fig. 11 Effect of amount of PANI/HY/5TiO$_2$ on the removal efficiency {$C_o=50$ ppm, $V=$ 50 ml and contact time 15 min}

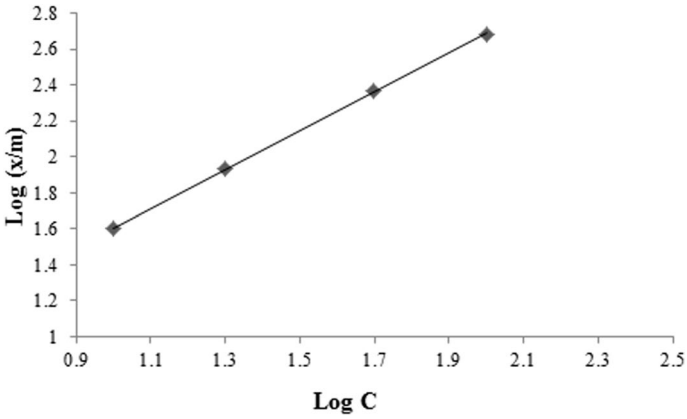

Fig. 12 Freundlich sorption isotherm {C_o = 50 ppm V = 50 mL and contact time = 15 min}

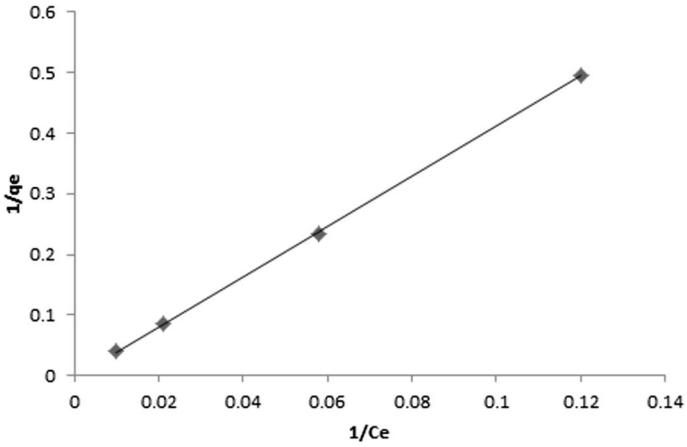

Fig. 13 Langmuir sorption isotherm {V = 50 ml and contact time = 15 min}

Effect of Cr(VI) concentration

The experimental results obtained at various concentrations show that the adsorption on the PANI/HY/5TiO_2 nanocomposite follows the Langmuir isotherm better than Freundlich one (Figs. 12 and 13). This isotherm is valid for monolayer adsorption onto a surface containing a finite number of identical sites.

The effect of Cr(VI) concentration on the uptake behavior of the PANI/HY/5TiO_2 nanocomposites was studied in the concentration range (10–100 ppm) (Fig. 12). Increasing the concentration enhances the percentage of loading. The adsorption coefficient K_{ad} of the composite for the Cr(VI) adsorption was computed from the Freundlich adsorption isotherm. Both isotherms (Langmuir and Freundlich) are represented by Eqs. (4) and (5), respectively [52].

$$\frac{C_e}{q_e} = \frac{1}{Q_0 b} + \frac{1}{Q_0} C_e \tag{4}$$

$$\ln q_e = \ln K_F + \frac{1}{n_F} \ln C_e \tag{5}$$

$$R_L = \frac{1}{\left(1 + bC_0\right)} \tag{6}$$

where C_e is the equilibrium Cr(VI) concentration and q_e the amount of Cr(VI) adsorbed at equilibrium (mg/g). The constant Q_o (mg/g) represents the monolayer adsorption capacity and b (L/mg) relates the adsorption heat.

R_L lies between 0 and 1 (Eq. 6) while the positive constant b indicates that the adsorption of Cr(VI) onto PANI/HY/5TiO_2 is favorable and the Langmuir model is suitable for fitting the experimental data. All R_L values obtained for Cr(VI) adsorption are between 0 and 1, indicating a favorable adsorption. n_F is an empirical parameter related to the intensity of adsorption, which varies with the heterogeneity of the adsorbent and values in the range (1–10), indicating a favorable adsorption [53–56].

The Freundlich isotherm is an indication of the surface heterogeneity of the adsorbent and is responsible for multilayer adsorption due to the presence of energetically heterogeneous adsorption sites. Greater the n_F value, better is the favorability of adsorption; the values of adsorbents are shown in Table 1.

Thermodynamic study

In order to evaluate the thermodynamic parameters for the adsorption of Cr(VI) onto PANI/HY/5TiO_2, the tests were carried out at three temperatures (299, 323 and 373 K). The standard free energy ($\Delta G°$) is the fundamental criterion of spontaneity, determined from the equilibrium constant (K_c):

$$\Delta G° = -RTLnK_c \tag{7}$$

where R is the universal gas constant (8.314 J mol^{-1} K^{-1}) and T the absolute temperature. The thermodynamic functions namely the standard enthalpy ($\Delta H◦$) and standard entropy ($\Delta S◦$) were determined from 399 to 373 K, using the relation:

Table 1 Adsorption isotherm for Cr(VI) removal adsorption onto the PANI/HY/5TiO_2

Langmuir constants				Freundlich constants		
Q_m (mg/g)	b (L/mg)	R^2	R_L	K_F (mg/g)	$1/n$	R^2
454.54	0.0108	0.999	0.65	2.957	0.5215	0.998

[a]The R_L value was obtained for the initial Cr (VI) concentration (C_o) of 50 mg/L

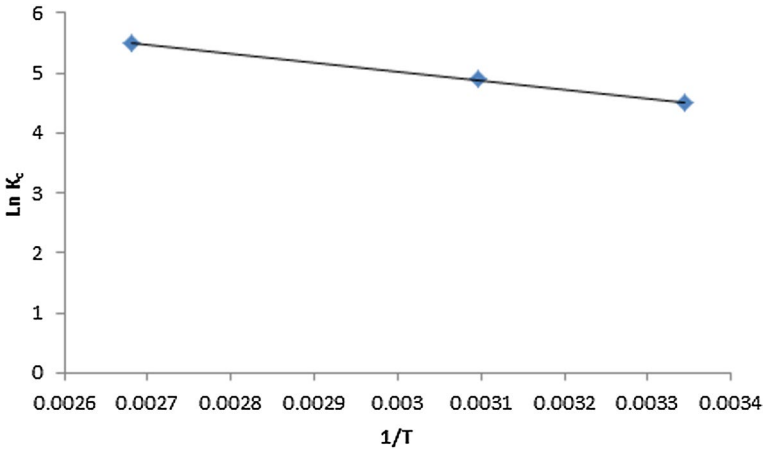

Fig. 14 Plot of Ln Kc versus 1/*T* for Cr(VI) adsorption onto PANI/HY/5TiO_2

Table 2 Thermodynamic data for Cr(VI) adsorption onto PANI/HY/5TiO_2

Temperature (*K*)	$\Delta G°$ (kJ/mol)	$\Delta H°$ (kJ/mol)	$\Delta S°$ (J/mol K)	R^2
299	− 11.186	12.478	79.2315	0.999
323	− 13.158			
373	− 17.056			

$$LnK_c = \frac{\Delta S^0}{R} - \frac{\Delta H^0}{RT}. \tag{8}$$

$\Delta H°$ and $\Delta S°$ are obtained from the slope and intercept of the linear plot of LnK_c versus 1/*T* (Fig. 14). The positive enthalpy $\Delta H◦$ indicates an endothermic Cr(VI) adsorption on PANI/HY/5TiO_2 while the negative value of $\Delta G◦$ reflects the feasibility and spontaneity of the adsorption and becomes more negative with increase in temperature.

$\Delta H°$ gives also information about the type of adsorption, i.e., physical (2–21 kJ mol^{-1}), chemical (21–418 kJ mol^{-1}) or physical–chemical [57, 58]. $\Delta H°$ for Cr(VI) adsorption onto PANI/HY/5TiO_2 was found to be 12.48 kJ mol^{-1} (Table 2), indicating the physical adsorption. This facilitates desorption for subsequent Cr(VI) removal cycles. Otherwise, the positive entropy (79.2315 J K^{-1} mol^{-1}) indicates an increase in randomness at the solid–solute interface during the adsorption [59, 60].

Conclusion

PANI/HY/TiO_2 nanocomposite was prepared by in situ polymerization method and the effect of acid solid (zeolite HY) with doped polyaniline is remarkable in the electrical conductivity. The interaction between PANI, zeolite HY and TiO_2 (anatase polymorph) was confirmed by FT-IR spectroscopy and XRD analysis, the latter showed nanosize range of PANI/HY/TiO_2.

The adsorption of PANI/HY/TiO_2 nanocomposite was successfully tested for the removal of chromate, a hazardous ion. The adsorption capacity onto PANI/HY/5TiO_2 nanocomposite increases with increasing the initial Cr(VI) concentration due to a high active surface area. The maximum adsorption capacity is found to be 454.54 mg/g at pH 7.3 and it is well classified than most reported polymer-based materials. The experimental isotherms were successfully fitted to the Langmuir isotherm model. The standard enthalpy change ($\Delta H°$) and incomplete desorption suggested a physical Cr(VI) adsorption, facilitating the recovery of PANI/HY/TiO2 for further adsorption cycles.

Acknowledgements This study was supported by the Faculty of Chemistry (USTHB, Algiers).

Declarations

Conflict of interest All the authors have no competing interests to declare.

References

1. Zhang J, Liu X, Wu S, Xu H, Cao B (2013) One-pot fabrication of uniform polypyrrole/Au nanocomposites and investigation for gas sensing. Sens Actuators B 186:695–700
2. Du Y, Shen SZ, Cai K, Casey PS (2012) Research progress on polymer–inorganic thermoelectric nanocomposite materials. Prog Polym Sci 37:820–841
3. Saranya S, Selvan RK, Priyadharsini N (2012) Synthesis and characterization of polyaniline/$MnWO_4$ nanocomposites as electrodes for pseudo capacitors. Appl Surf Sci 258:4881–4887
4. Rajesh, Ahujab T, Kumar D (2009) Recent progress in the development of nano-structured conducting polymers/nanocomposites for sensor applications. Sens Actuators B 136:275–286
5. Zhu CL, Chou SW, He SF, Liao WN, Chen CC (2007) Synthesis of core/shell metal oxide/polyaniline nanocomposites and hollow polyaniline capsules. Nanotechnology 18(275604):1–6
6. Ram MK, Yavuz O, Lahsqngah V, Aldissi M (2005) CO gas sensing from ultrathin nano-composite conducting polymer film. Sens Actuators B 106:750–757
7. Liangchao L, Haizhen Q, Yuping W, Jing J, Feng X (2008) Preparation and magnetic properties of $Cu_{0.4}Zn_{0.6}Cr_{0.5}Sm_{0.06}Fe_{1.44}O_4$/polyaniline nanocomposites. J Rare Earths 26(4):558–562
8. Fusalba F, Bélanger D (1999) Chemical synthesis and characterization of polyaniline-molybdenum trisulfide composite. J Mater Res 14:1805–1813
9. Huang J (2006) Syntheses and applications of conducting polymer polyaniline nanofibers. Pure Appl Chem 78:15–27
10. Li L, Yan Z (2005) Synthesis and characterization of self-assembled V_2O_5 mesostructures intercalated by polyaniline. J Nat Gas Chem 14:35–39
11. Li Y, Gong J, He G, Deng Y (2011) Fabrication of polyaniline/titanium dioxide composite nanofibers for gas sensing application. Mater Chem Phys 129:477–482
12. Sun L, Shi Y, He Z, Li B, Liu J (2012) Synthesis and characterization of SnO_2/polyaniline nanocomposites by sol-gel technique and microemulsion polymerization, Synthetic. Metal 162:2183–2187

13. Sadek AZ, Wlodarski W, Shin K, Kaner RB, Kalantar-zadeh K (2008) A polyaniline/WO_3 nanofiber composite-based ZnO/64◦ YX LiNbO3SAW hydrogen gas sensor. Synth Met 158:29–32
14. Patil SL, Chougule MA, Sen S, Patil VB (2012) Measurements on room temperature gas sensing properties of CSA doped polyaniline–ZnO nanocomposites. Measurement 45:243–249
15. Ravikiran YT, Lagare MT, Sairam M, Mallikarjuna NN, Sreedhar B, Manohar S, MacDiarmid AG, Aminabhavi TM (2006) Synthesis, characterization and low frequency AC conduction of polyaniline/niobium pentoxide composites. Synth Met 156:1139–1147
16. Shankarananda AL, Kalyani S (2012) Chemical oxidation method for synthesis of polyaniline–In_2O_3 composites. Int J Eng Sci 1(10):59–64
17. Choi SG, Lee SH (1999) Preliminary molecular dynamic simulation studies of H-Y zeolite in a non-rigid zeolite framework. Bull Korean Chem Soc 20:445–450
18. Pansini M, Colella C (1990) Dynamic data on lead uptake from water by chabazite. Desalination 78:287–295
19. Albino V, Cioffi R, Pansini M, Colella C (1995) Disposal of lead-containing zeolite sludges in cement matrix. Env Technol 16:147–165
20. Baerlocher Ch, Meier WM, Olson DH (2001) Atlas of zeolite framework types. Elsevier, Amsterdam, pp 132–133
21. Ellis J, Korth W (1993) Removal of geosmin and methylisoborneol from drinking water by adsorption on ultra-stable zeolite-Y. Water Res 4:535–539
22. Chen SS, Taylor JS, Mulford LA (2004) Influences of molecular weight molecular size, flux, and recovery for aromatic pesticides removal by nanofiltration membranes. Desalination 160:103–111
23. Malkaj P, Dalas E, Vitoratos E, Sakkopoulos S (2006) pH electrodes constructed from polyaniline/zeolite and polypyrrole/zeolite conductive blends. J Appl Polym Sci 101:1853–1856
24. Tabet L, Zougar M, Djebbouri S, Sali S, Kermadi O, Mahroua A, Mahieddine M (2022) Trari, Photo-electrochemical properties of nanostructured metal-semiconductor Al/TiO_2 thin film. Appl Rhodamine B Oxidation Under Sunlight Optik 249:168288
25. Wang F, Min S, Han Y, Feng L (2010) Visible-light-induced photocatalytic degradation of methylene blue with polyaniline-sensitized TiO2 composite photocatalysts. Superlattices Microstruct 48:170–180
26. Li Y, Yua Y, Wua L, Zhi J (2013) Processable polyaniline/titania nanocomposites with good photocatalytic and conductivity properties prepared via peroxo-titanium complex catalyzed emulsion polymerization approach. Appl Surf Sci 273:135–143
27. Jo WK, Kang HJ (2013) (Ratios: 5, 10, 50, 100, and 200) Polyaniline TiO_2 composites under visible- or UV-light irradiation for decomposition of organic vapors, Mater Chem Phys, 1–9
28. Kang Q, Lu QZ, Liu SH, Yang LX, Wen LF, Luo SL, Cai QY (2010) A ternary hybrid CdS/Pt-TiO_2 nanotube structure for photoelectrocatalytic bactericidal effects on Escherichia Coli. Biomaterials 31:3317–3326
29. Zubillaga O, Cano FJ, Azkarate I, Molchan IS, Thommpson GE, Cabral AM, Morais PJ (2008) Corrosion performance of anodic films containing polyaniline and Tio2nanoparticles on AA3105 aluminium alloy. Surf Coat Technol 202:5936–5942
30. Gong J, Li Y, Hu Z, Zhou Z, Deng Y (2010) Ultrasensitive NH_3 Gas Sensor from Polyaniline Nanograin Enchased TiO_2 Fibers. J Phys Chem C 114:9970–9974
31. Rahmani AR, Samadi MT, Noroozi R (2011) Hexavalent chromium removal from aqueous solutions by adsorption onto synthetic nano size ZeroValent Iron (nZVI), world academy of science. Eng Technol 50:80–83
32. Selvi K, Pattabhi S, Kadirvelu K (2001) Removal Cr(VI) from aqueous solution by adsorption onto carbon. Biores Technol 80:87–89
33. Okparanma RN, Ayotamuno MJ (2008) Predicting chromium (VI) adsorption rate in the treatment of liquid-phase oil-based drill cuttings. African J Environ Sci Technol 2(4):068–074
34. Gholipour M, Hashemipour H, Mollashahi M (2011) Hexavalent chromium removal from aqueous solution via adsorption on granular activated carbon: adsorption desorption, modeling and simulation studies. ARPN J Eng Appl Sci 6(9):10–18
35. Wanga PC, Venancio EC, Sarno DM, MacDiarmid AG (2009) Simplifying the reaction system for the preparation of polyaniline nanofibers: Re-examination of template-free oxidative chemical polymerization of aniline in conventional low-pH acidic aqueous media. React Funct Polym 69:217–223

36. Wang J, Zhang K, Zhaoa L, Ma W, Liu T (2014) Adsorption and polymerization of aniline on a carboxylic group-modified fibrous substrate. Synth Met 188:6–12
37. Yan J, Wang C, Gao Y, Zheng Z, Zhong S, Miao X, Cui X, Wang H (2011) Anchoring conductive polyaniline on the surface of expandable polystyrene beads by swelling-based and in situ polymerization of aniline method. Chem Eng J 172:564–571
38. Safidin Z, Ghebache Z, Lamouri S (2013) thermoelectrical characterization of new material bases on PANI/Zeolite HY composite used for detection of carbon dioxide, Polymer J, 1–9
39. Tamboli MS, Kulkarni MV, Patil RH, Gade WN, Navale SC, Kale BB (2012) Nanowires of silver–polyaniline nanocomposite synthesized via in situ polymerization and its novel functionality as an antibacterial agent. Colloids Surf, B 92:35–41
40. Wu Z, Chen X, Zhu S, Yao Y, Guo H (2013) Effect of humidity on electrical properties of micro/nano-polyaniline thin films with different D-CSA doping degree. Measurement 46:411–419
41. Xuan Z, Lu L (2011) Facile synthesis of 1-(N-butyl-1,8-naphthalimide-4′-yl)-3-(4-methoxylphenyl)-5-phenyl-pyrazoline/polyaniline core–shell nanofibers and polyaniline nanotubes. Mater Lett 65:754–756
42. Ayad M, El-Hefnawy G, Zaghlol S (2013) Facile synthesis of polyaniline nanoparticles; its adsorption behavior. Chem Eng J 217:460–465
43. Chen H, Matsumoto A, Nishimiya N, Tsutsumi K (1999) Preparation and characterization of TiO2 incorporated. Colloids Surf Physicochem Eng Aspects 157:295–305
44. Alwash AH, Abdullah AZ, Ismail N (2013) TiO_2-zeolite Y catalyst prepared using impregnation and ion-exchange method for sonocatalytic degradation of amaranth dye in Aqueous solution, World Academy of Science. Eng Technol 78:782–790
45. Bulakhe RN, Patil SV, Deshmukh PR, Shinde NM, Lokhande CD (2013) Fabrication and performance of polypyrrole (Ppy)/TiO_2 heterojunction for room temperature operated LPG sensor. Sens Actuators B 181:417–423
46. Zhang L (2007) Electrochemical synthesis of self-doped polyaniline and its use to the electrooxidation of ascorbic acid. J Solid State Electrochem 11:365–371
47. Thanpitcha T, Sirivat A, Jamieson AM, Rujiravanit R (2009) Polyaniline nanoparticles with controlled sizes using a cross-linked carboxymethyl chitin template. J Nanopart Res 11:1167–1177
48. Ram MS, Palaniappan S (2004) A process for the preparation of polyaniline salt doped with acid and surfactant groups using benzoyl peroxide. J Mater Sci 39:3069–3077
49. Farias RF, Nunes LM (2002) Thermogravimetric study about PVC-polyaniline blends. J Therm Anal Calorim 70:559–564
50. Jian SS, Noriyuki K (2000) Processable polyaniline titanium dioxide nanocomposites: effect of titanium dioxide on the conductivity. Synth Met 114:147–153
51. Denga F, Li Y, Luo X, Yang L, Tu X (2011) Preparation of conductive polypyrrole/TiO2 nanocomposite via surface molecular imprinting technique and its photocatalytic activity under simulated solar light irradiation, Colloids Surfaces A: Physicochem Eng Aspects xxx: 1–7.
52. Shia T, Wang Z, Liub Y, Jia S, Changming D (2009) Removal of hexavalent chromium from aqueous solutions by D301, D314 andD354 anion-exchange resins. J Hazardous Mater 161:900–906
53. Hena S (2010) Removal of chromium hexavalent ion from aqueous solutions using biopolymer chitosan coated with poly 3-methyl thiophene polymer. J Hazardous Mater 181:474–479
54. Samani MR, Borghei SM, Olad A, Chaichi MJ (2010) Removal of chromium from aqueous solution using polyaniline – Poly ethylene glycol composite. J Hazardous Mater 184:248–254
55. Bhaumik M, McCrindle R, Maity A (2013) efficient removal of Congo red from aqueous solution by adsorption onto interconnected polypyrrole-polyaniline nanofibres. Chem Eng J 228:506–515
56. Kumar R, Ansari MO, Barakat MA (2013) DBSA doped polyaniline/multi-walled carbon nanotubes composite for high efficiency removal of Cr(VI) from aqueous solution. Chem Eng J 228:748–755
57. Muhammad A, Shah AU, Bilal S (2019) Comparative study of the adsorption of acid blue 40 on polyaniline, magnetic oxide and their composites: synthesis, characterization and application. Materials 12(18):2854
58. X. Hoa Vu, L. H. Nguyen, H. T. Van, D. V. Nguyen, T. H. Nguyen, Q. T. Nguyen, L. T. Ha (2019) Adsorption of chromium(VI) onto freshwater snail shell-derived biosorbent from aqueous solutions: equilibrium, kinetics, and thermodynamics, J Chem, 1–11.
59. Harrache Z, Abbas M, Aksil T, Trari M Thermodynamic and kinetics studies on adsorption of Indigo Carmine from aqueous solution by activated carbon

60. Moussa M, Trari M (2020) Contribution of adsorption and photo catalysis for the elimination of Black Eriochrome (NET) in an aqueous medium-Optimization of the parameters and kinetics modelling. Sci African 8:e00387

Authors and Affiliations

Z. Ghebache[1] · Z. Safidine[2] · F. Hamidouche[3] · N. Boudieb[3] · A. Benaboura[1] · M. Trari[4]

[1] Laboratoire de Synthèse Macromoléculaire et Thio-Organique Macromoléculaire, Faculté de Chimie, USTHB, Algiers, Algeria

[2] Macromolecular Chemistry Laboratory, EMP, PO 17, 16111 Bordj-El-Bahri CityAlgiers, Algeria

[3] Processing and Formatting Fibrous Polymers Laboratory (LTMFPF), Faculty of Engineering, University M'hamed Bougara, Boumerdes, Algeria

[4] Laboratory of Storage and Valorization of Renewable Energies LSVER, Faculty of Chemistry, USTHB, BP 32, 16111 Algiers, Algeria